Journal of Physics: Conference Series

Ultracold collisions in the Yb-Li mixture system

Ultracold collisions in the Yb-Li mixture system

Florian Schäfer[1], Hideki Konishi[1], Adrien Bouscal[2], Tomoya Yagami[1], Matthew D Frye[3], Jeremy M Hutson[3] and Yoshiro Takahashi[1]

[1] Department of Physics, Graduate School of Science, Kyoto University, Kyoto 606-8502, Japan
[2] Département de Physique, École Normale Supérieure, PSL Research University, 24 rue Lhomond, 75005 Paris, France
[3] Joint Quantum Centre (JQC) Durham-Newcastle, Department of Chemistry, University of Durham, South Road, Durham, DH1 3LE, United Kingdom

E-mail: schaefer@scphys.kyoto-u.ac.jp

Abstract. We report our experimental results on the collisional physics between non-S-state atoms (ytterbium (Yb), effectively a two-electron system, in the metastable $^3P_2$ state) and S-state atoms (lithium (Li), an alkali metal, in the ground state). At low magnetic fields, by measuring inelastic interspecies collisional losses in the double quantum degenerate mixture we reveal the strong dependence of the inelastic losses on the internal spin states of both species and suppressed losses in stretched state configurations. Increasing the magnetic field up to 800 G we further investigate the magnetic field dependence of the collisional interactions. There, smoothly increasing inelastic losses are observed towards higher fields. The combined knowledge of both the magnetic field and the spin state dependence of the collisional losses of this prototypical mixture system of non-S-state and S-state atoms provides a significant step forward towards controllable impurity physics realized in the Yb-Li ultracold system.

1. Introduction

The understanding and control of the collisional properties of single-species ultracold atomic systems was and is instrumental to their application in the research of fundamental phenomena, quantum simulation and quantum computation. For example, elastic collisions enable us to reach ultracold temperatures via forced evaporative cooling [1], light-assisted collisions lead in photo-association processes to molecular states [2], manipulation of the scattering lengths by means of Feshbach resonances [3] facilitate the crossover from Bose-Einstein condensates to Bardeen–Cooper–Schrieffer superfluids [4, 5] and give insight to Efimov trimer physics [6], and controlled collisions between atoms form one possible basis for quantum gates in quantum computation schemes [7].

Going from single-species to two-species systems adds additional degrees of freedom to the experimental toolkit. For example, the physics of impurity systems leads to questions of both transport and localization of quantum matter [8, 9, 10]. Related questions in mixed dimensional systems range from basic phase diagram considerations [11] to the possibility of chiral p-wave superfluids [12, 13] and their application to topologically protected quantum computation [14, 15]. Also, polar molecules associated from two-species ultracold mixtures allow implementation of novel spin-lattice models as new platforms for quantum computation protocols [16].

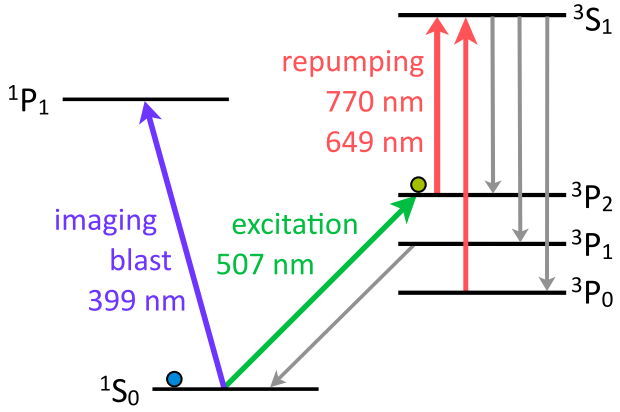

Figure 1. Yb level scheme of relevance to the experiments. Light at 507 nm connects the ground to the metastable $^3P_2$ state (green arrow). Fluorescence imaging at the strong $^1S_0 - {}^1P_1$ transition (purple arrow) reveals the remaining $^3P_2$ atoms after a blast of any remaining ground state atoms and transfer of the excited atoms to the ground state by two repumping lasers (red arrows) followed by spontaneous decay (gray arrows).

We here present and summarize our experiments on quantum degenerate mixtures of fermionic ^{6}Li and bosonic ^{174}Yb, where Yb is in the metastable $^3P_2$ state (see Fig. 1). First, at low magnetic bias fields we investigate inelastic interspecies collisional losses in the double quantum degenerate mixture that reveal the dependence of the inelastic losses on the internal spin states of both species. As a result, we discover two very distinct regimes: in collisions with ^{6}Li in the $F = 1/2$ hyperfine state overall constant inelastic collision rates are found. These results are in agreement with our previous report [17]. The collisional system with ^{6}Li in the $F = 3/2$ state, however, exhibits quite a different behavior. Now the magnetic sublevel of ^{174}Yb matters and we observe suppressed losses for stretched state configurations and up to 40-times increased relaxation rates in the other cases. Second, we measure the magnetic field dependence of the inelastic collision rates between ^{174}Yb, again in the metastable $^3P_2$ state, and ^{6}Li for several hyperfine levels of Li. Those experiments reveal a smooth but steady increase of the inelastic collision rates up to the highest investigated magnetic fields of 800 G and underline the importance of choosing collisional channels with suppressed inelastic dynamics.

This Progress Report is organized as follows: After this introduction we will review the necessary experimental details in Sec. 2. The individual results are then presented and explained in Sec. 3 and Sec. 4. Section 5 concludes the Report with a summary and a general discussion of our experimental findings.

2. Experiment

We here review the necessary experimental methods that are also discussed in more depth and detail in the related works [18, 19, 20]. Starting from a hot beam of thermal Yb and Li atoms from a dual-species oven, both species are sequentially Zeeman slowed and trapped in a magneto-optical trap (MOT). The atomic beam contains abundances of all stable isotopes of both species. By proper selection of the laser frequencies we choose to to slow down and cool only selected isotopes, namely bosonic ^{174}Yb and fermionic ^{6}Li. From the MOT the pre-cooled samples are transferred to a crossed far-off-resonant trap (FORT) created by two focused laser beams at wavelengths of about 1060 nm. Next, the intensities of the FORT lasers are decreased as to drive forced evaporative cooling of the ^{174}Yb atoms until quantum degeneracy, a Bose-Einstein condensate (BEC), is reached. Our setup is not designed to perform evaporative cooling of Li independently. Instead, Li is in thermal contact with Yb and is cooled to quantum degeneracy via sympathetic cooling [21].

During the initial phase of the evaporative cooling ramp we apply a 0.5 ms pulse of circularly polarized light resonant to either the Li $F = 1/2 \rightarrow F' = 1/2$ or the $F = 3/2 \rightarrow F' = 3/2$ D1-line transition. Together with a repumping light derived from the D2-line MOT light lasers we can effectively prepare a spin-polarized ^{6}Li sample in either of the four $F = 1/2$, $m_F = \pm 1/2$

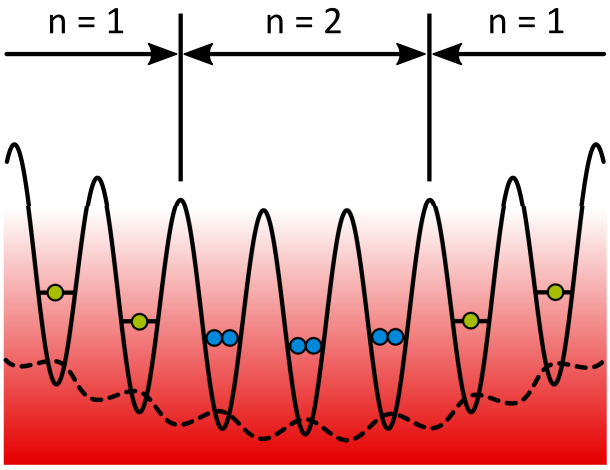

Figure 2. Quantum degenerate mixture of ^{174}Yb and ^{6}Li in a 3D optical lattice. Yb experiences a deep lattice potential (solid line) and forms a Mott-insulator shell structure (blue and green dots, only occupations numbers $n \leq 2$ shown). The effective potential for Li is shallow (dashed line) and the atoms remain unlocalized (red shaded area). For our investigation of inter-species scattering we focus on the interaction between ^{6}Li and ^{174}Yb(^{3}P$_2$) atoms (green dots) in $n = 1$ sites.

or $F = 3/2$, $m_F = \pm 3/2$ ground states. This polarization state remains with high fidelity until quantum degeneracy is reached and time-of-flight absorption imaging after application of a strong magnetic field gradient reveals above 90% of final spin-polarization. By choosing appropriate loading durations for the ^{174}Yb and ^{6}Li MOTs at this point we typically obtain a BEC of 10×10^4 ^{174}Yb atoms and a Fermi degenerate ^{6}Li gas of 3×10^4 atoms. The temperature of Li is about 300 nK or about 0.2 T_F, where T_F is the Fermi temperature. Typical densities at this point are 5×10^{14} cm^{-3} for ^{174}Yb and 5×10^{12} cm^{-3} for ^{6}Li.

As we want to study the collisional dynamics between non-S-state atoms (^{174}Yb in the metastable ^{3}P$_2$ state) and S-state atoms (spin-polarized ^{6}Li in the ground state) it is necessary (i) to prepare the Yb atoms in the ^{3}P$_2$ state and (ii) to prevent fast losses stemming from inelastic Yb(^{3}P$_2$)-Yb(^{3}P$_2$) collisions [22]. To both ends we adiabatically load the quantum degenerate mixture into a three-dimensional (3D) optical lattice, formed by three pairs of counter-propagating laser beams of wavelength $\lambda_\mathrm{L} = 532$ nm. At λ_L the sign of the polarizabilities of Li and Yb are opposite. The chosen lattice depths are about 15 E_R^Yb for ^{174}Yb and 0.7 E_R^Li for ^{6}Li, where E_R^Yb (E_R^Li) is the recoil energy of Yb (Li). Hence, while ^{6}Li only experiences a minor modulation of its wave function ^{174}Yb forms a Mott-insulator state (see Fig. 2 and Refs. [23, 17]). The difference in gravitational sag of the two species is addressed by an additional light field gradient, increasing the otherwise small spatial overlap between ^{174}Yb and ^{6}Li [17].

Using pairs of magnetic coils in Helmholtz configuration we then apply the desired bias fields, typically between 100 mG and 800 G. There, the metastable ^{3}P$_2$ state of Yb experiences significant Zeeman splitting of 2.1 MHz/G$\times m_J$. By application of a 0.5 ms long pulse of 507-nm light resonant to the ^{1}S$_0$ - ^{3}P$_2$ transition we then site and state selectively excite ^{174}Yb atoms only in singly occupied lattice sites ($n = 1$) and for a desired target Zeeman state $-2 \leq m_J \leq 2$. This effectively suppresses Yb(^{3}P$_2$)-Yb(^{3}P$_2$) collisional events. The excitation strength is chosen such that the number of excited ^{174}Yb atoms is about 10% of the total number of ^{6}Li atoms. In the following we can therefore assume that there is only a small number of non-S-state ^{174}Yb atoms immersed within a large Fermi sea of S-state ^{6}Li atoms. After the excitation a short light pulse at 399 nm removes the remaining ground state ^{174}Yb atoms from the system, ensuring no contributions from ground state Yb atoms to our results. During a variable holding time we then allow the excited ^{174}Yb atoms to interact with the background ^{6}Li gas. We note that losses of excited-state atoms due to collisions with hot background gas atoms and scattering from the trap lasers limit the lifetime of the ^{3}P$_2$ atoms to (850 ± 300) ms which is much longer than the typical timescales involved in interactions with ^{6}Li.

In the detection stage of the experiment we measure the remaining ^{174}Yb(^{3}P$_2$) atoms via the very sensitive fluorescence imaging method on the strong 399-nm transition (see Fig. 1 and

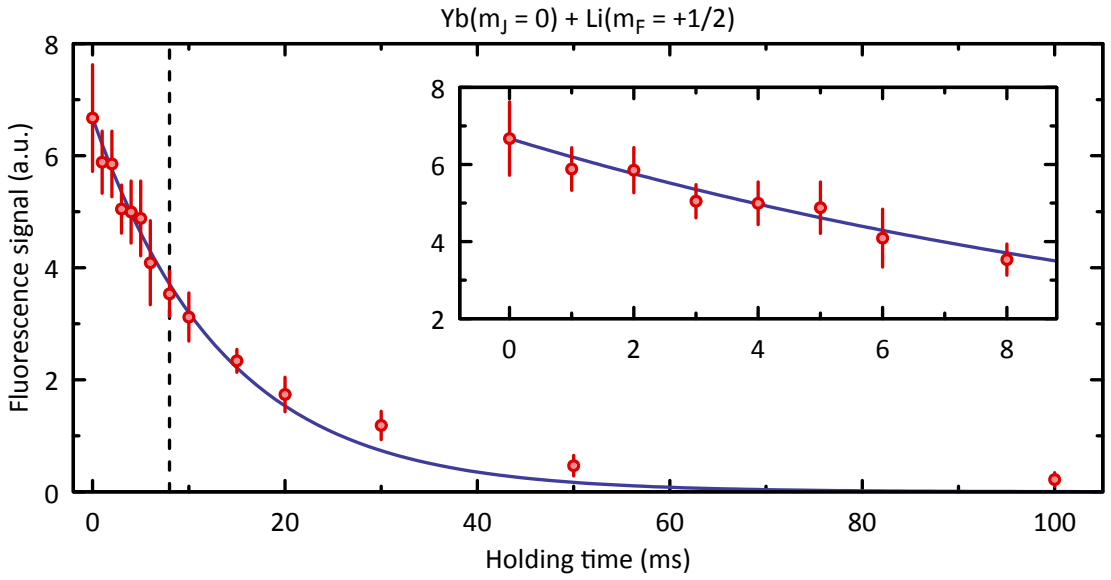

Figure 3. Decay of ^{174}Yb(^{3}P$_2, m_J = 0$) excited state atoms through inelastic collisions with ^{6}Li(^{2}S$_{1/2}, F = 1/2, m_F = +1/2$) ground state atoms, where we show the intensity of the obtained fluorescence signal as a function of the holding time. The data points (red) are the mean of independent measurements at each holding time. The error bars represent their standard deviations. An exponential decay (blue, solid line) is fitted to the initial time window (up to the dashed line) and shown enlarged in the inset. The lifetime obtained here is (13.5 ± 1.2) ms corresponding to an inelastic collisional rate coefficient of $(4.6 \pm 2.2) \times 10^{-11}$ cm^3/s.

Ref. [17]). For this we first apply a 399-nm light pulse to remove any accumulated ^{174}Yb(^{1}S$_0$) atoms from the system, followed by a short pulse of two repumping lasers (cf. Fig. 1) that transfers the remaining ^{174}Yb(^{3}P$_2$) atoms back to the ground state. There they are recaptured by a MOT operating on the 399-nm transition whose fluorescence light is integrated for 1 s on a sensitive charge-coupled device (CCD) camera to obtain a high-contrast signal of the MOT proportional to the number of ^{174}Yb(^{3}P$_2$) atoms. Imaging of the ^{6}Li atoms proceeds via standard time-of-flight absorption imaging.

3. Spin dependence

A first series of experiments is to establish the dependence of the inelastic collisions on the spin state of both the non-S-state ^{174}Yb(^{3}P$_2$) and the S-state ^{6}Li(^{2}S$_{1/2}$) collisional partners. This is to gain more insight into anisotropy induced relaxation processes [24, 25, 26] in this collisional process.

The experiment proceeds as outlined in Sec. 2. During the first 100 ms of the adiabatic increase of the optical lattice depth we set a homogeneous bias magnetic field of 200 mG. This is to define a good quantization axis and to lift the degeneracy of the five $m_J = -2, \ldots, +2$ Zeeman states of ^{174}Yb(^{3}P$_2$). The experiment is executed for all combinations of Yb Zeeman states and accessible Li ground states, 20 configurations in total. For each combination we repeat the experiment several times, varying each time the holding time of the mixture in the optical lattice up to 100 ms. We point out that at the present bias magnetic field we could confirm that our method is sensitive to fine-structure changing collisions (e.g. Yb(^{3}P$_2$) $\rightarrow$ Yb(^{3}P$_1$)) and hyperfine-structure changing collisions ($F = 3/2 \rightarrow F = 1/2$). In contrast, spin-changing collisions (m_J or m_F change) do not lead to sufficient gain in kinetic energy for the atoms to

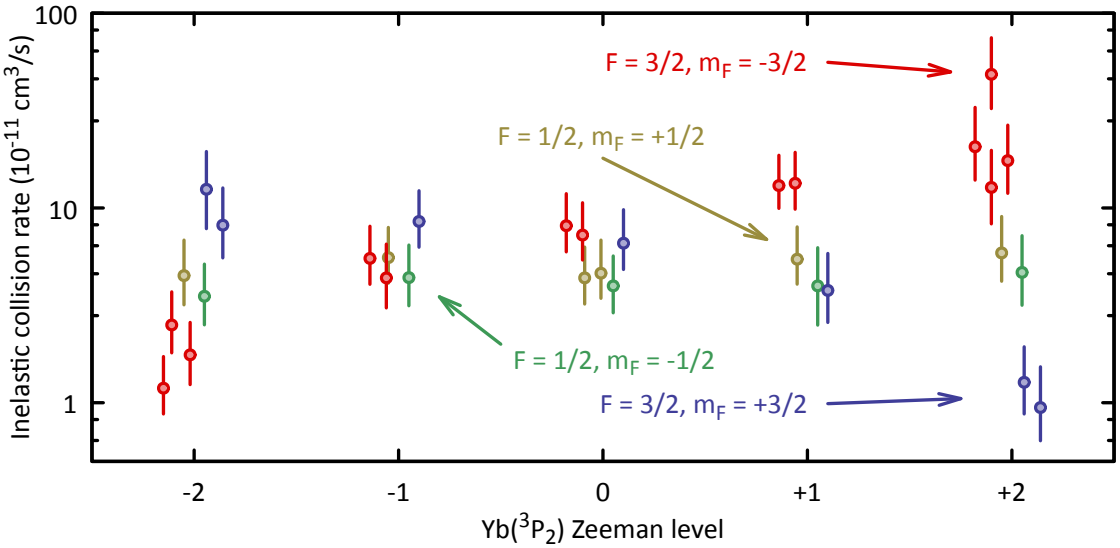

Figure 4. Inelastic collision rates between metastable ^{174}Yb(^{3}P$_2$) and ground state ^{6}Li in various hyperfine states at 200 mG bias magnetic field. Inelastic collisions with ^{6}Li(^{2}S$_{1/2}, F = 1/2, m_F = \pm 1/2$) (yellow and green symbols) show only a weak dependence on the m_J magnetic state of ^{174}Yb. In contrast, a clear m_J-state dependence in collisions with ^{6}Li(^{2}S$_{1/2}, F = 3/2, m_F = \pm 3/2$) is observed (blue and red symbols). The data points represent the median values, the error bars the $1-\sigma$ confidence interval of the determined collision rates. The data are slightly shifted horizontally for better visibility.

leave the optical lattice [19].

A representative decay of the remaining ^{3}P$_2$ atoms is shown in Fig. 3. The data qualitatively can be divided into two decay regimes. An initial, faster decay is followed by a slower decay dynamics. Having confirmed the linearity of our fluorescence light detection system, we interpret this as the crossover from a decay mostly governed by interspecies collisions to a mixed dynamics where also collisions of the Yb(^{3}P$_2$) atoms with background gas atoms combined with slightly reduced Li densities gain importance. We therefore typically limit the analysis of the data to the first few milliseconds (indicated by the dashed line and the inset in Fig. 3). The initial decay is then analyzed in terms of rate equations taking Yb(^{3}P$_2$)-Li inelastic losses and Yb(^{3}P$_2$) one-body losses into account. The details of the numerical analysis are described in our related work [19]. The analysis then gives access to a lifetime τ that, with knowledge of the atomic densities and their overlap, is translated into the inelastic loss parameter.

Figure 4 summarizes the results of this survey. The data fall into two categories. Looking at intermediate collisional rates we observe that the data for collisions with ^{6}Li(^{2}S$_{1/2}, F = 1/2, m_F = \pm 1/2$) all have very similar inelastic loss rates of about 4×10^{-11} cm^3/s. Collisions with ^{6}Li in the $F = 3/2$ hyperfine state, however, show a very pronounced and systematic dependence on the magnetic sublevel of both ^{174}Yb(^{3}P$_2$) and ^{6}Li. Especially for collisions between ^{174}Yb(^{3}P$_2, m_J = +2$) and ^{6}Li(^{2}S$_{1/2}, F = 3/2, m_F = \pm 3/2$) a 40-fold change of the loss rate is observed.

The findings are discussed in terms of the interspecies interaction operator $\hat{U}$ described in detail for the Yb(^{3}P$_2$)-Li(^{2}S$_{1/2}$) system in [27]. The anisotropy introduced into $\hat{U}$ by the non-S-state species leads to significant differences in the potentials of the four possible Yb(^{3}P$_2$)-Li(^{2}S$_{1/2}$) molecular states [28] and drives strong, spin dependent relaxation processes [26].

Indeed our inelastic loss rates are generally several orders of magnitude larger than those reported for systems where the anisotropy is suppressed by screening effects of outer s-shell orbitals [29]. The efficient suppression of inelastic losses observed in the configurations ^{174}Yb(^{3}P$_2, m_J = +2$)-^{6}Li(^{2}S$_{1/2}, F = 3/2, m_F = +3/2$) and ^{174}Yb(^{3}P$_2, m_J = -2$)-^{6}Li(^{2}S$_{1/2}, F = 3/2, m_F = -3/2$) stems from the lack of allowed inelastic decay channels for these stretched state configurations, assuming conservation of the total electronic angular momentum and its projection. According to [30] one can identify two contributions to $\hat{U}$, internal and external anisotropy. The internal anisotropy conserves the total electronic angular momentum and its projection. It therefore cannot cause inelastic changes in stretched state situations. In contrast, the external anisotropy couples to the rotational momentum of the nuclei and does not abide by the above conservation rule. In this light, our stretched state results allow direct access to the contribution by the external anisotropy that with inelastic collision rates of about 10^{-11} cm^3/s is in good agreement with earlier predictions [27]. The impact of the internal anisotropy is expressed by our findings for the non-stretched collisional systems where losses increase by one order of magnitude.

In order to understand the patterns of inelastic collision rates, we perform coupled-channel scattering calculations on Li+Yb(^{3}P$_2$). We use the same methods as described in Ref. [27], with all three spin-orbit states of Yb(^{3}P) included. The interaction potential for this system is known only from electronic structure theory [31] and is not accurate enough for quantitative predictions of scattering lengths or resonance predictions, but it should adequately represent the qualitative behaviour of the system. In order to sample the effects of different scattering lengths for the different electronic states, we construct 10 different interaction potentials. Each of these potentials is composed of 4 potential curves ($^2\Sigma^+$, $^2\Pi$, $^4\Pi$, and $^4\Sigma^+$), each of which is multiplied by a random scaling factor that varies over a range sufficient to randomise the scattering length of that potential completely.

We calculate loss rates at 200 mG for all 20 combinations of states for the experimental results shown in Fig. 4, for all 10 of our random potentials. There is a large variation of about 2 orders of magnitude in the overall magnitude of the loss rates between different potentials. This range encompasses the experimental results. For most interaction potentials, there is an approximate symmetry between calculated loss rates for (m_F, m_J) and $(-m_F, -m_J)$, although there are often differences of up 20%. Among the states of Li with $F = 1/2$, the differences between the loss rates for different Zeeman components are generally small, in agreement with the experiment.

For several of the potentials there is strong suppression of the loss rates for the spin-stretched states. Losses from these states require a change in L, the quantum number for end-over-end rotation, and so depend on the external anisotropy. In one view, this anisotropy is proportional to the difference between Σ and Π potentials. However, there may sometimes be a coincidental cancellation of the couplings, leading to suppression of loss from these states for some of our potentials. This cancellation may be conceptually similar to alkali-alkali systems with similar singlet and triplet scattering lengths [32, 33], where spin exchange is suppressed, but the details in this case are likely to be much more complicated. From the experimental results, it appears that the real system also exhibits this suppression.

4. Magnetic field dependence

We now turn our attention to the magnetic field dependence of the inelastic loss rates. Field strengths up to 800 G are considered. For field strengths > 300 G we directly ramp up the field, similar to the previous experiment, to the final value while preparing the optical lattice. For magnetic fields below 300 G, due to technical constraints of our setup, direct excitation is not efficiently possible. Instead we prepare and excite the sample at 300 G and then ramp down the field within 0.3 ms to the desired target field. Due to the strong Zeeman splitting of the Yb(^{3}P$_2$) state, the inevitable technical noise of the magnetic field and the narrow linewidth of

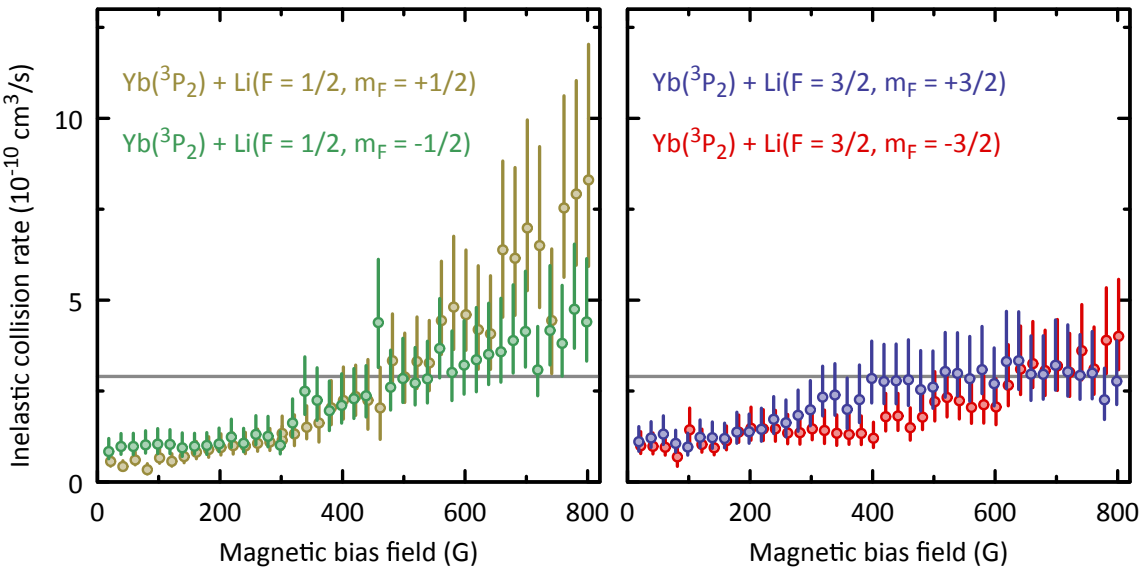

Figure 5. Summary of inelastic collision rates between ^{174}Yb(^{3}P$_2, m_J = 0$) and ^{6}Li(^{2}S$_{1/2}$) state atoms for bias magnetic fields between 20 and 800 G. The ^{6}Li atoms are either prepared in one of the two available $F = 1/2$ states (left panel) or the accessible $F = 3/2$ states (right panel). For easier comparison both panels are drawn to the same scale. Also indicated is the expected universal rate (gray lines). In all cases a smooth increase of the inelastic collision rate is found. No strong, resonance-like features indicative of possible Feshbach resonances are observed. The data is slightly offset horizontally for better readability.

the transition, we can reliably excite only the ^{174}Yb(^{3}P$_2, m_J = 0$) in this situation. Therefore, we limit this experiment to the $m_J = 0$ Zeeman state of ^{174}Yb(^{3}P$_2$). The data analysis is as in the low-field measurements of the preceding section.

The results are summarized in Fig. 5. Note, that even in this high-field situation we identify the states of Li by their low-field quantum numbers (F, m_F) at which they were prepared and that are adiabatically connected to the projections of the electronic and nuclear spin angular momenta (m_S, m_I) at high magnetic field. By using non-stretched state configurations the data include effects from both internal and external anisotropy and therefore should give a good overview of the general high-field behavior of the inelastic collisional loss rates. For all investigated spin states of ^{6}Li we find a smooth and general increase of the losses, starting with low fields at about 10^{-10} cm^3/s and staying below 10^{-9} cm^3/s when reaching 800 G. Especially for fields beyond about 600 G collisions involving ^{6}Li in the $F = 3/2$ hyperfine state have slightly lower losses then those with ^{6}Li in the $F = 1/2$ state. Overall, we find larger inelastic collisional rates than what was predicted in [27] for collisions involving Yb(^{3}P$_2, m_J = -2$). Also, for higher magnetic fields the losses approach and go beyond the predicted universal rate [27] of 2.9×10^{-10} cm^3/s (gray lines in Fig. 5); this corresponds to a model in which incoming flux can be reflected from the long-range potential, but all the flux that reaches short range is irreversibly lost with unit probability. [34]. This again exemplifies the importance of the anisotropy in $\hat{U}$ for ultracold collisions of ^{174}Yb(^{3}P$_2$) and ^{6}Li(^{2}S$_{1/2}$).

We have carried out further coupled-channel calculations to understand these results. We use the same interaction potentials as in the previous section, but now perform calculations up to 1000 G for the states shown in Fig. 5. The general behavior of the loss rates for these states is to increase from a small value at low field towards the universal loss rate [34], sometime rising above it at higher fields. There is resonant structure in most cases, which creates large peaks

in loss rate. Some of which can have widths of hundreds of Gauss and are responsible for rates higher than universal. Many of the resonant features appear consecutively in the three lowest spin channels for Li ($F = 1/2, m_F = 1/2$; $F = 1/2, m_F = -1/2$; $F = 3/2, m_F = -3/2$; all of which correspond to electron spin $m_s = -1/2$) at progressively higher field, most likely due to a single state cutting upwards in energy through each of the thresholds in turn. Turning to the experimental results, the loss rates in the lowest Li channel ($F = 1/2\, m_F = 1/2$) rise strongly towards the upper end of the field range. The loss rates in the next states up rise less strongly, but one of them is still clearly above the universal rate. This behavior may be evidence of a broad resonance in the loss rate, centered above 800 G for the $F = 1/2, m_F = 1/2$ channel, and at even higher fields for the higher $F = 1/2, m_F = -1/2$ and $F = 3/2, m_F = -3/2$ channels. Further measurements at higher fields would be able to confirm if this is indeed the case.

5. Conclusions

We investigated the inelastic rates in the ^{174}Yb(^{3}P$_2$)-^{6}Li(^{2}S$_{1/2}$) system of non-S-state and S-state collisional partners. In contrast to S-state-only collisions effects of anisotropy become of significant importance here. This is evidenced by the strong dependence on the spin states we observed at low magnetic fields. At higher magnetic fields we find inelastic collision rates beyond the universal rate of complete loss at short distances. Furthermore only a smooth variation of the loss rates is found. While the general findings are supported by our coupled-channel calculations, the details are as yet mostly beyond our understanding. This renders experimental investigations all the more important and should encourage further theoretical studies. It would for example be interesting to extend our high-field studies to the numerically more investigated case of ^{174}Yb(^{3}P$_2, m_J = -2$) that might prove to be more collisionally stable.

In future experiments towards controllable impurity physics in the ultracold Yb-Li mixture system consideration of the anisotropy and its associated additional losses is necessary and stretched-state configurations should be preferred where possible to suppress unnecessary loss mechanisms. Our work thus provides a significant step towards a better understanding and control of ultracold Yb(^{3}P$_2$)-Li mixtures.

Acknowledgments

We thank Ruth Le Sueur for useful early discussions. This work was supported by the Grant-in-Aid for Scientific Research of JSPS Grants No. JP25220711, No. JP26247064, No. JP16H00990, No. JP16H01053, No. JP17H06138, No. 18H05405, No. 18H05228, JST CREST Grant No. JPMJCR1673, the Impulsing Paradigm Change through Disruptive Technologies (ImPACT) program by the Cabinet Office, Government of Japan, and MEXT-QLEAP. Further support was provided by U.K. Engineering and Physical Sciences Research Council (EPSRC) Grant No. EP/P01058X/1. HK achnowledges support from JSPS.

References

[1] Ketterle W and Druten N V 1996 *Advances In Atomic, Molecular, and Optical Physics* vol Volume 37 ed Benjamin Bederson and Herbert Walther (Academic Press) pp 181–236 ISBN 1049-250X
[2] Weiner J, Bagnato V S, Zilio S and Julienne P S 1999 *Rev. Mod. Phys.* **71** 1–85
[3] Chin C, Grimm R, Julienne P and Tiesinga E 2010 *Rev. Mod. Phys.* **82** 1225
[4] Bourdel T, Khaykovich L, Cubizolles J, Zhang J, Chevy F, Teichmann M, Tarruell L, Kokkelmans S J J M F and Salomon C 2004 *Phys. Rev. Lett.* **93** 050401
[5] Zwierlein M W, Stan C A, Schunck C H, Raupach S M F, Kerman A J and Ketterle W 2004 *Phys. Rev. Lett.* **92** 120403
[6] Zaccanti M, Deissler B, D'Errico C, Fattori M, Jona-Lasinio M, Müller S, Roati G, Inguscio M and Modugno G 2009 *Nature Physics* **5** 586–591 ISSN 1745-2473
[7] Daley A J 2011 *Quantum Information Processing* **10** 865–884 ISSN 1570-0755, 1573-1332
[8] Massignan P, Zaccanti M and Bruun G M 2014 *Rep. Prog. Phys.* **77** 034401 ISSN 0034-4885
[9] Chien C C, Peotta S and Ventra M D 2015 *Nat. Phys.* **11** 998–1004 ISSN 1745-2481

[10] Nishida Y 2016 *Phys. Rev. A* **93** 011606
[11] Nishida Y and Tan S 2008 *Phys. Rev. Lett.* **101** 170401
[12] Nishida Y 2009 *Annals of Physics* **324** 897–919 ISSN 0003-4916
[13] Wu Y J, He J, Zang C L and Kou S P 2012 *Phys. Rev. B* **86** 085128
[14] Kitaev A Y 2003 *Annals of Physics* **303** 2–30 ISSN 0003-4916
[15] Tewari S, Das Sarma S, Nayak C, Zhang C and Zoller P 2007 *Phys. Rev. Lett.* **98** 010506
[16] Micheli A, Brennen G K and Zoller P 2006 *Nat. Phys.* **2** 341–347 ISSN 1745-2473
[17] Konishi H, Schäfer F, Ueda S and Takahashi Y 2016 *New J. Phys.* **18** 103009 ISSN 1367-2630
[18] Hara H, Takasu Y, Yamaoka Y, Doyle J M and Takahashi Y 2011 *Phys. Rev. Lett.* **106** 205304
[19] Schäfer F, Konishi H, Bouscal A, Yagami T and Takahashi Y 2017 *New J. Phys.* **19** 103039 ISSN 1367-2630
[20] Schäfer F, Konishi H, Bouscal A, Yagami T and Takahashi Y 2017 *Phys. Rev. A* **96** 032711
[21] Myatt C J, Burt E A, Ghrist R W, Cornell E A and Wieman C E 1997 *Phys. Rev. Lett.* **78** 586–589
[22] Uetake S, Murakami R, Doyle J M and Takahashi Y 2012 *Phys. Rev. A* **86** 032712
[23] Bloch I, Dalibard J and Zwerger W 2008 *Rev. Mod. Phys.* **80** 885–964 ISSN 0034-6861
[24] Reid R H G and Dalgarno A 1969 *Phys. Rev. Lett.* **22** 1029–1030
[25] Mies F H 1973 *Phys. Rev. A* **7** 942–957
[26] Krems R V, Kłos J, Rode M F, Szcześniak M M, Chałasiński G and Dalgarno A 2005 *Phys. Rev. Lett.* **94** 013202 ISSN 0031-9007, 1079-7114
[27] González-Martínez M L and Hutson J M 2013 *Phys. Rev. A* **88** 020701
[28] Petrov A, Makrides C and Kotochigova S 2015 *New J. Phys.* **17** 045010 ISSN 1367-2630
[29] Hancox C I, Doret S C, Hummon M T, Krems R V and Doyle J M 2005 *Phys. Rev. Lett.* **94** 013201 ISSN 0031-9007, 1079-7114
[30] Krems R V, Groenenboom G C and Dalgarno A 2004 *J. Phys. Chem. A* **108** 8941–8948 ISSN 1089-5639
[31] Gopakumar G, Abe M, Das B P, Hada M and Hirao K 2010 *J. Chem. Phys.* **133** 124317 ISSN 0021-9606
[32] Julienne P S, Mies F H, Tiesinga E and Williams C J 1997 *Phys. Rev. Lett.* **78** 1880–1883
[33] Burke J P, Bohn J L, Esry B D and Greene C H 1997 *Phys. Rev. A* **55** R2511–R2514
[34] Idziaszek Z and Julienne P S 2010 *Phys. Rev. Lett.* **104** 113202